Biochimica et Biophysica Acta 1818 (2012) 1726–1736

Contents lists available at SciVerse ScienceDirect

Biochimica et Biophysica Acta

journal homepage: www.elsevier.com/locate/bbamem

Coupling between the voltage-sensing and pore domains in a voltage-gated potassium channel

Eric V. Schow [a], J. Alfredo Freites [a], Alex Nizkorodov [a], Stephen H. White [b,c], Douglas J. Tobias [a,c,*]

[a] Department of Chemistry, University of California, Irvine, CA 92697-2025, USA
[b] Department of Physiology and Biophysics, University of California, Irvine, CA 92697-4560, USA
[c] Center for Biomembrane Systems, University of California, Irvine, CA 92697-4560, USA

ARTICLE INFO

Article history:
Received 3 November 2011
Received in revised form 24 February 2012
Accepted 28 February 2012
Available online 9 March 2012

Keywords:
Ion channel
Voltage-gating
Molecular dynamics simulation
Membrane protein

ABSTRACT

Voltage-dependent potassium (Kv), sodium (Nav), and calcium channels open and close in response to changes in transmembrane (TM) potential, thus regulating cell excitability by controlling ion flow across the membrane. An outstanding question concerning voltage gating is how voltage-induced conformational changes of the channel voltage-sensing domains (VSDs) are coupled through the S4–S5 interfacial linking helices to the opening and closing of the pore domain (PD). To investigate the coupling between the VSDs and the PD, we generated a closed Kv channel configuration from *Aeropyrum pernix* (KvAP) using atomistic simulations with experiment-based restraints on the VSDs. Full closure of the channel required, in addition to the experimentally determined TM displacement, that the VSDs be displaced both inwardly and laterally around the PD. This twisting motion generates a tight hydrophobic interface between the S4–S5 linkers and the C-terminal ends of the pore domain S6 helices in agreement with available experimental evidence.

1. Introduction

Kv channels are tetramers with a modular architecture consisting of four peripheral voltage-sensing domains (VSDs) and one central pore domain (Fig. 1). Each Kv monomer consists of a VSD, comprised four TM helices (S1–S4), that is loosely linked to the pore domain, which consists of two TM helices (S5, S6) and the selectivity filter. The voltage-sensitivity of the channel is conferred by the highly conserved S4 sequence in which basic residues (usually Arg) occur at every third position, separated by two hydrophobic residues (Fig. 2). The VSDs observed in open-state Kv structures are in the so-called "up state" in which the S4 charges are close to the extracellular side of the membrane [1]. The trajectory and range of motion of the S4 helix during gating have been debated extensively, but it is generally accepted that, when the channel is closed, the VSDs adopt a "down-state" configuration in which the S4 charges are closer to the intracellular side. Mechanical coupling between the VSDs and the pore domain is responsible for gating the channel [2]. We explore in this paper the structural restraints of the coupling required for channel closure.

X-ray crystal structures of three different Kv channels in an open state have been reported [1,3–5]. A structure of a Nav channel mutant was recently reported [6] in which the VSDs are apparently in the up state, but the pore is closed due to engineered disulfide bridges near the opening of the intracellular gate. To date, no structures have been reported for a fully closed voltage-gated ion channel (i.e., with a closed pore and down-state VSDs). The lack of structures has hindered understanding the molecular mechanism of voltage gating at the atomic level. To gain insights into the coupling between the voltage-sensing and pore domains during channel gating, we have generated a model of the KvAP channel in the closed state based entirely on the motions of the VSDs.

Comparison of the three open-state Kv channel crystal structures with those of non voltage-gated prokaryotic channels in both open and closed conformations [7–12], as well as functional data has established firmly that the α-helical bundle-crossing formed by the C-terminal halves of the four S6 segments constitutes the activation gate in Kv channels (reviewed by Swartz [11] and Tombola et al. [12]). Opening and closing of this gate may involve an absolutely conserved glycine residue in the middle of S6 that is essential to channel biogenesis and function [13,14]. This glycine is thought to enable a hinge-bending motion during gating [7]. The actual coupling between VSDs and the pore domain occurs at a second site where the S6 helices bend to allow for the interaction with the S4–S5 linker [1,2,15–17]. This second site is less conserved among Kv channels, and may correspond to a Pro residue that is part of the PXP (X = V,I) motif in the Kv1 through Kv4 subfamilies, or a Gly residue, as in the case of the prokaryotic KvAP (Fig. 2).

The VSD is an independent structural and functional unit [5,16,18–20]; homologs of Kv VSDs act independently as a proton channel [21,22] and as a voltage-sensitive phosphatase [23] lacking a pore domain. We recently reported a model for the isolated KvAP VSD in a down state [24] based on the biotin–avidin accessibility data of Ruta et al. [25] that provided a quantitative, one-dimensional (1D) spatial

* Corresponding author at: Department of Chemistry, University of California, Irvine, Irvine, CA 92697-2025, USA. Tel.: +1 949 824 4295; fax: +1 949 824 9920.
E-mail address: dtobias@uci.edu (D.J. Tobias).

0005-2736/$ – see front matter © 2012 Elsevier B.V. All rights reserved.
doi:10.1016/j.bbamem.2012.02.029

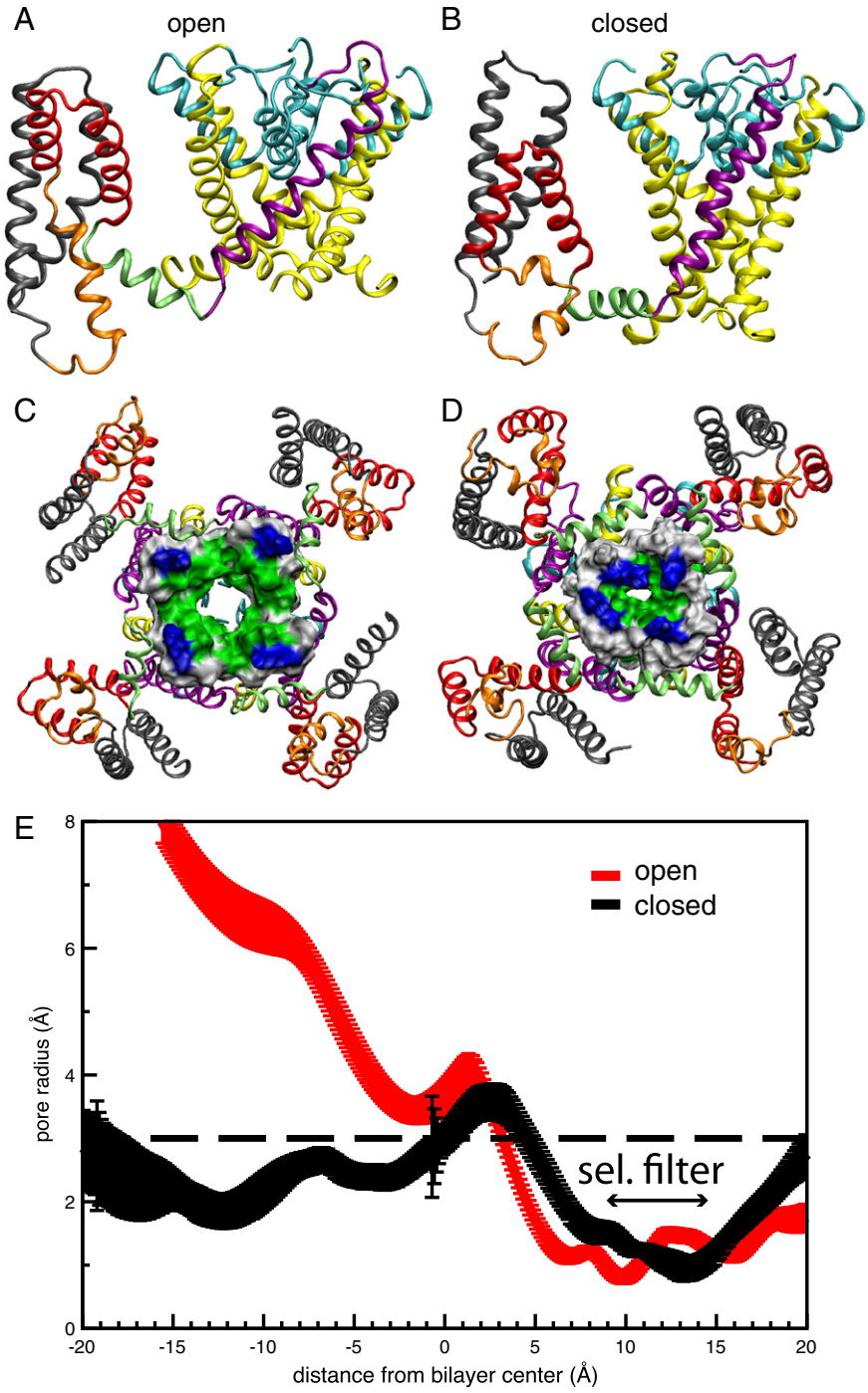

Fig. 1. The KvAP channel in an open and a closed state. (A,B) Side views of the pore domain and a single voltage sensor in the open and closed states, respectively. S1 and S2 are gray; S3a, orange; S3b–S4, red; S4–S5 linker, green; S5 purple; P-helix, cyan; S6, yellow. (C,D) View from the intracellular side of the open and closed channels, respectively. The intracellular half of S6 is shown in reduced-surface representation with nonpolar residues colored white; polar residues colored green; and basic residues colored blue. (E) Pore radius profiles for the unrestrained open and closed state trajectories (~270 ns each) along the transmembrane (TM) direction (i.e., membrane normal). Distances along the TM direction are measured from the center of the lipid bilayer. Error bars are +/− one standard deviation.

description of the VSD motions during activation. Here we extend our modeling to include the full KvAP channel in order to explore the coupling between the VSDs and the pore domain. To this end, we used targeted molecular dynamics (TMD) simulations, during which restraint forces were applied only to the VSDs so that any changes in the pore domain structure are due solely to mechanical coupling between the pore domain and the VSDs. We find that, in addition to motion along the TM direction, lateral motions of the VSDs are required to produce a closed configuration of the pore domain. Through prolonged unrestrained atomistic simulations of both the open and closed states under the influence of appropriate transmembrane potentials produced by ionic gradients, we characterize the structural changes that lead to the closing of the pore domain, and assign putative roles in the activation gating mechanism to the two conserved glycine residues in S6. We identify a fully developed hydrophobic interface between the S4–S5 linkers and the C-termini of S6 segments in the closed state as the main structural feature that establishes the mechanical coupling between the VSDs and the pore domain.

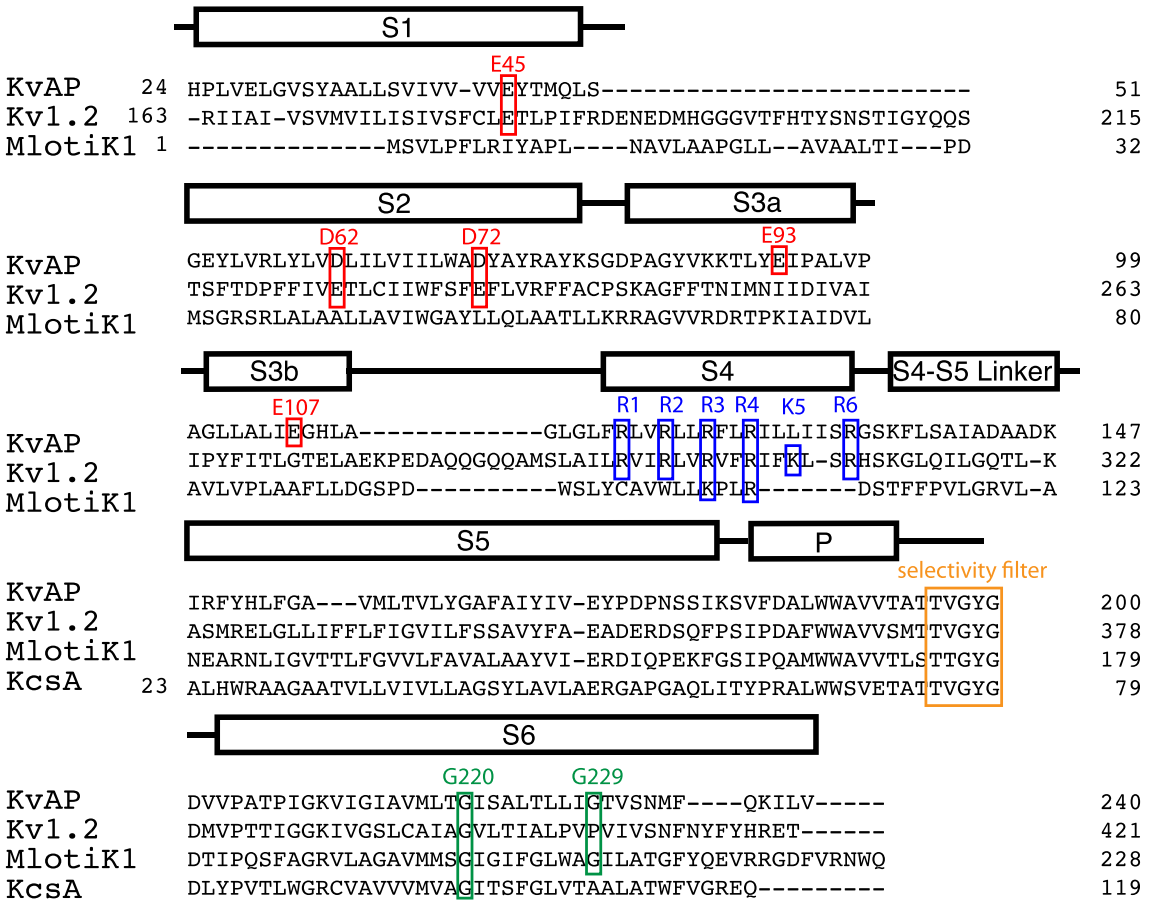

Fig. 2. Sequence alignments of KvAP, Kv1.2, KcSA, and MlotiK1. Several key acidic residues are boxed in red, the conserved S4 basic residues in blue, the selectivity filter in orange, and the important S6 glycines in green. Labeled residues are numbered according to the KvAP sequence, except for the S4 basic residues, which are labeled according to the standard R1–R6 numbering scheme (K5 is not present in KvAP). The alignment was performed using the National Center for Biotechnology Information (NCBI) COBALT Multiple Alignment Tool with some manual adjustments.

2. Methods

2.1. Molecular dynamics simulations

All simulations were performed with the NAMD 2.7b2 software package [26]. The CHARMM22 and CHARMM32 force fields [27,28] were used for the protein and lipids, respectively, and the TIP3P model was used for water [29]. The smooth particle mesh Ewald method [30,31] was used to calculate electrostatic interactions. Short-range real-space interactions were cut off at 11 Å, employing a switching function. A reversible multiple time-step algorithm [32] was employed to integrate the equations of motion with a time step of 4 fs for electrostatic forces, 2 fs for short-range non-bonded forces, and 1 fs for bonded forces. All bond lengths involving hydrogen atoms were held fixed using the SHAKE [33] and SETTLE [34] algorithms. Molecular graphics and trajectory analyses were performed using VMD 1.8.7 [35]. A Langevin dynamics scheme was used for temperature control and a Nosé–Hoover–Langevin piston was used for pressure control [36,37]. Pore radius measurements were performed with HOLE 2.2 [38]. Continuum electrostatic calculations were performed using the CHARMM 32a2 software package [39], as described elsewhere [24].

2.1.1. Open state

The initial configuration of the open state model consisted of the full KvAP channel model proposed by Lee et al. [4] embedded in a POPC bilayer (780 lipids) in excess water (47,847 water molecules). Three crystallographic K^+ ions, two at sites S3 and S1 in the selectivity filter and one in the internal vestibule, were held fixed throughout the simulation. The total number of atoms, including 11 chloride counterions, was 260,827. The initial equilibration consisted of 2000 steps of energy minimization, followed by a 200 ps run at constant volume and temperature (300 K) with the protein backbone held fixed. The protein was then progressively released from its initial configuration over 600 ps using harmonic restraints. The simulation was run unrestrained for 11.5 ns at constant temperature and pressure (1 atm) prior to applying harmonic restraints to the T47 and V183 C_α atoms which are reported to be in closed contact as part of a evolutionarily-conserved interface between the VSDs S1 segments and the pore domain [40]. The T47–V183 restraint force constants were progressively increased over 5 ns to a value of 16 kcal mol^{-1} $Å^{-2}$. The system was then run for 10 ns, after which the restraints were released over five 1 − ns intervals.

After releasing the T47–V183 restraints, we allowed the system to relax for 10 ns, and we then placed it in an ionic solution such that the TM potential corresponded to roughly 100 mV, extracellular relative to intracellular, which is approximately the biological depolarized potential. In order to perform our simulation under a realistic electrostatic potential, we followed the protocol of Treptow et al. [41]. We isolated the intracellular and extracellular ionic solutions by doubling the simulation box size in the *z*-direction to 180 Å, thus creating a solution-vacuum interface on both sides of the system, which enabled us to maintain an ionic imbalance across the membrane. The net ionic imbalance was such that the intracellular ionic solution contained an additional $+3e$. The system was then run at constant temperature (300 K) and volume for 270 ns.

2.1.2. Closed state

The closed state model was generated using targeted molecular dynamics as implemented in NAMD [26]. In a TMD simulation, forces are applied simultaneously to a collection of atoms, according to the following potential:

$$U = \frac{k}{2N}\left(RMS(t) - RMS^{*}(t)\right)^2$$

where k is the collective force constant, N is the number of targeted atoms, $RMS(t)$ is the actual root-mean-square distance (RMSD) between the current (at time t) and target configurations, and $RMS^{*}(t)$ evolves from the RMSD between the initial and target configurations toward the desired final RMSD (in this case, zero).

Four different TMD runs were performed using the same initial configuration from the equilibrated open-state trajectory. Each target configuration consisted of the same opened pore domain as in the initial configuration surrounded by four symmetrically placed down-state VSDs [24]. The target configurations differed only in the position of the VSDs in the membrane plane with respect to the initial configuration, as depicted in Fig. 3. Forces were applied to 1188 heavy atoms, including the S1–S4 backbone atoms, the side chains of E28, E45, D62, D72, E107, and the S4 Args, to encourage the formation of salt-bridges as seen in the isolated VSD model [24]. Each TMD run was performed over 10 ns using a per-atom force constant (k/N) of 2.02 kcal mol^{-1} Å^{-2}. A fifth TMD run was performed with this target configuration, but using an initial open-state configuration that did not include the S1-pore restraints between T47 and V183. The RMSD between the initial and each target configurations was ~12 Å. Of these TMD runs, one resulted in a

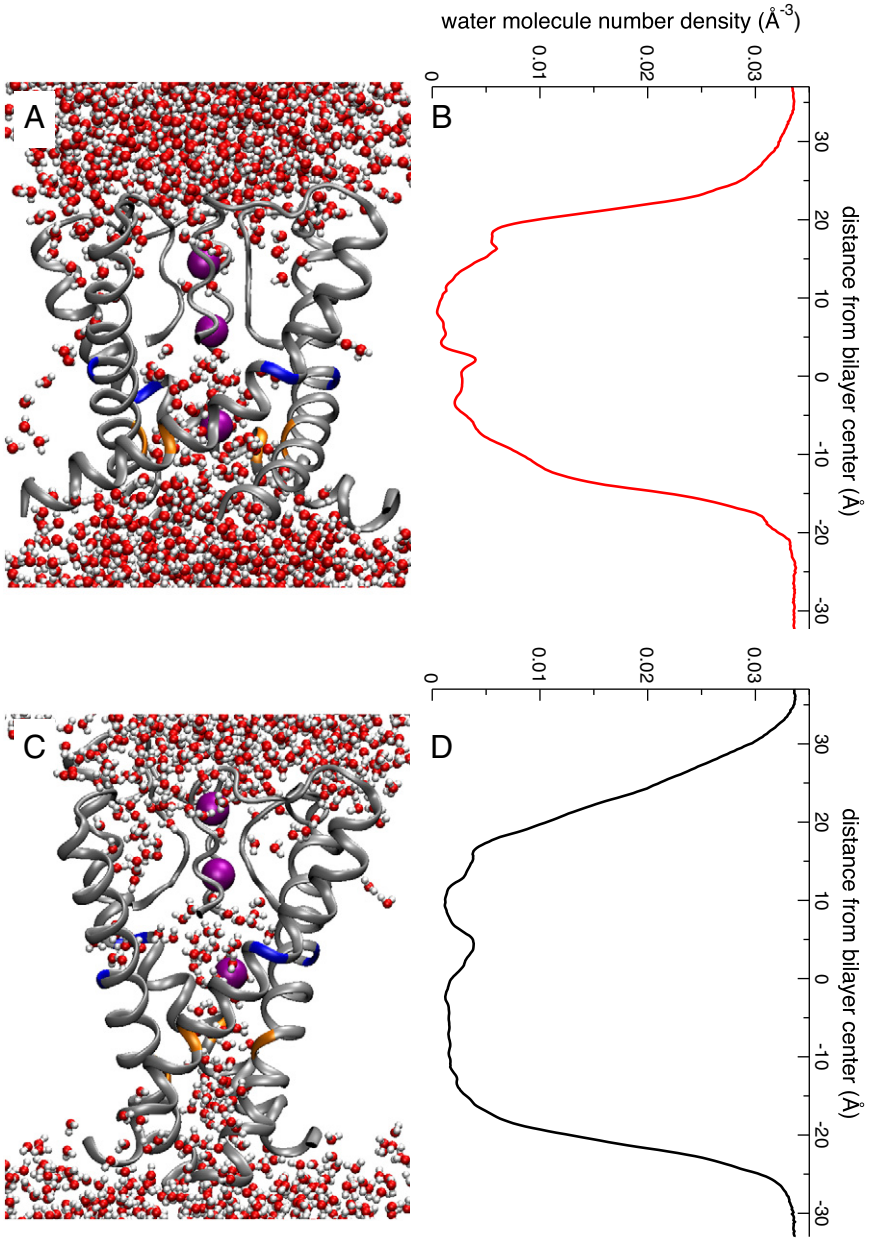

Fig. 3. Hydration of the KvAP pore. (A,C) Snapshots of the open and closed pore domains, respectively. S6 and the selectivity filter are shown as gray ribbons. The locations of G220 (blue) and G229 (orange) on S6 are highlighted as colored ribbon. K^+ ions are shown as purple spheres and the waters in the cylindrical region defined by the pore domain are colored by atom (oxygen, red; hydrogen, white). (B,D) Water number–density profiles along the TM direction in the region of the open and closed pore domains, respectively. The hydrated inner vestibule, located just below the selectivity filter, is clearly visible in the closed-state water density profile.

configuration that appeared to be fully closed, which was determined by measuring of the pore radius (Fig. 4F, S4C).

The endpoint of the TMD simulation that generated a fully closed pore domain was used as the basis for an extended MD simulation. The last configuration was placed in a 150 mM ionic solution (as described above for the open state configuration) with a hyperpolarized TM potential of −100 mV. The net ionic imbalance was such that the extracellular ionic solution contained an additional +3*e*. This configuration was then run at constant temperature (300 K) and volume for 280 ns.

2.2. Comparison to biotin–avidin accessibility data

The biotin–avidin accessibility assay employed by MacKinnon and coworkers [25,42] relies on the principle that biotin, tethered to a specific residue, can only be captured by avidin at the lipid bilayer interface. Thus, to verify that our simulation trajectories for both the up and down states conform to the biotin–avidin accessibility data, we assumed that for a biotinylated residue to be accessible to avidin, the position of its Cα atom along the TM direction, measured from the lipid bilayer interface, should be within the effective length of the tether[25]. To define the bilayer interfaces for comparison of distances to the Ruta et al. data [25], we used the mean positions of the lipid carbonyl distributions; ~15.5 Å from the system center with a FWHM of ~7 Å (see Fig. S1). Because the biotin–avidin binding event does not distinguish between conformations of the VSD, we assumed that a given residue would be accessible if the specific effective tether length was within the bounds defined by the minimum and maximum Cα position in either trajectory. The results, shown in

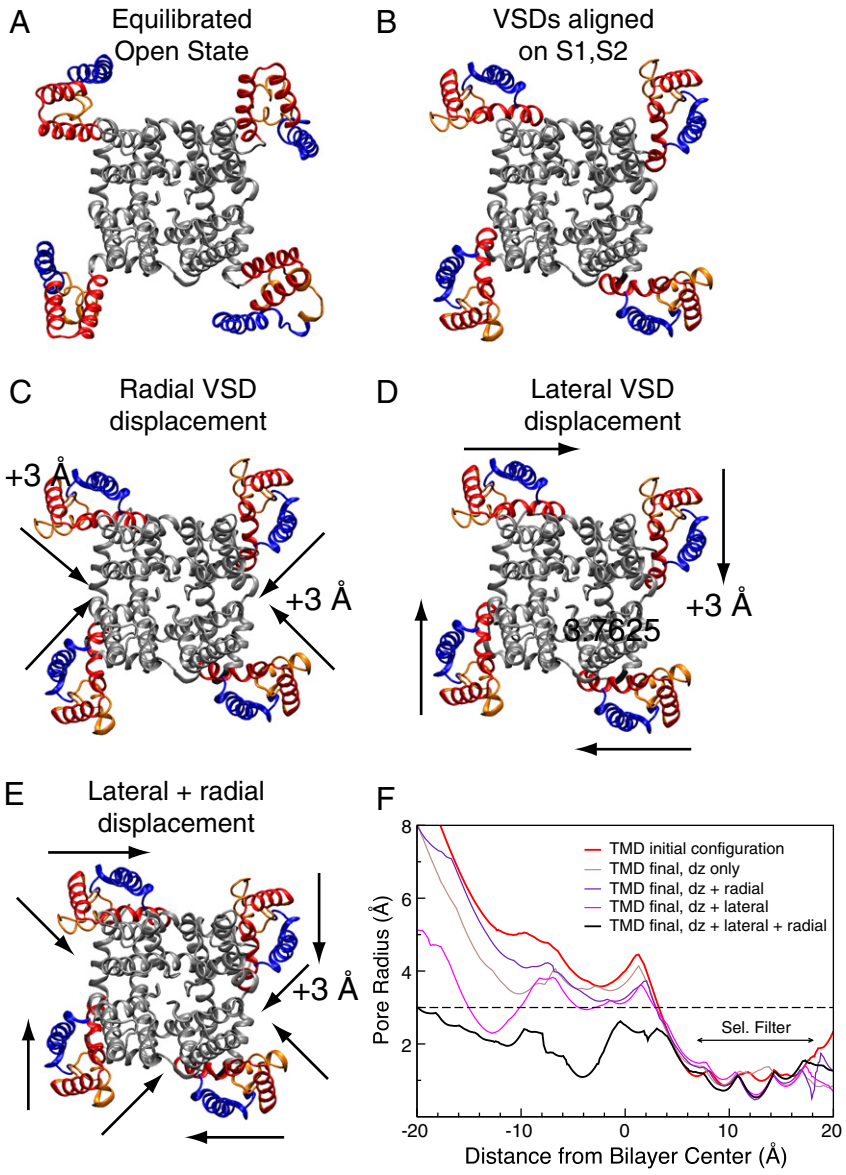

Fig. 4. Summary of the targeted molecular dynamics (TMD) target configurations. The down state of the isolated KvAP VSD [24] defines the position of the VSD only along the TM direction. Consequently, four different target states were tried in which the VSD positions differed in their placement relative to the PD. (A) Initial open-state configuration. (B) This target configuration consists of the same pore domain as in the initial configuration flanked by four down state VSDs [24]. The S1–S2 segments in both initial and target configurations were fitted to each other so that there was no net displacement of the VSDs in the plane of the membrane between the initial and final configurations. (C) Each target VSD was displaced 3 Å inwardly. (D) Each target VSD was displaced 3 Å around the pore domain in the plane of the membrane as indicated by the arrows. (E) The target VSDs were subject to both a lateral (clockwise) and an inward displacement both 3 Å in magnitude. In addition to the VSD TM motion, our results show that the combination of some inward and clockwise displacements on the membrane plane are necessary to close the channel via coupling between the S4–S5 linker and the intracellular half of S6. (F) Pore radius profiles calculated for the open KvAP channel (red line) and at the end of each of the TMD runs. The dashed black line represents the nominal radius of a hydrated K^+ ion. A fully closed pore resulted only when lateral and radial restraints were applied simultaneously (solid black line).

Fig. 6, suggest that, overall, the Cα positions in the equilibrated trajectories are consistent with the biotin–avidin accessibility data.

The biotin–avidin accessibility data for the KvAP VSD indicate that only the voltage-sensor paddle (S3b–S4) and the S4–S5 linker are mobile along the TM direction [25,42]. This allowed Ruta et al. [25] to estimate a range of 29–34 Å for the hydrocarbon core thickness based on accessibility measurements in the S1 and S2 segments and the pore domain (S5 segment). These estimates are in good agreement with the location of the lipid carbonyl group in our simulations (+/− 15.5 Å) and can be considered to reflect the thermal disorder in the fluid lipid bilayer. The accessibility results from the simulation and the accessibility experiment do not agree for a small subset of residues even when the width of the carbonyl distributions (FWHM of ~7 Å) is taken into account. However, the assumption that the location of the lipid bilayer interface (i.e., the location of the avidin molecule) and the effective tether length are independent of residue position can introduce enough uncertainty to account for these discrepancies, setting aside issues of force field accuracy or the validity of the biotin–avidin reaction as a reliable assay for accessibility. If, for example, instead of taking the mean of the carbonyl distributions as a measure of the extent of penetration of avidin into the polar region of the lipid bilayer, we take the mean phosphate position, nearly all of the discrepancies outside of the S3b–S4 motif vanish. On the other hand, discrepancies within S3b–S4 follow the opposite trend, i.e., they assume a shorter span for the hydrocarbon core, which is consistent with the notion that the outermost charges in S4 are solvated by the lipid phosphate groups, creating a local distortion of the bilayer [20].

3. Results

We performed 270 ns unrestrained simulations of the KvAP tetramer in both open (Fig. 1A,C) and closed (Fig. 1B,D) conformations in a lipid bilayer in excess water. The open-state simulation, based on the full-channel model reported by Lee et al. [4], was equilibrated with additional restraints to form contacts between the extracellular ends of S1 and the pore domain, as suggested by Lee et al. [40].

3.1. Closing the channel requires a torque on the S4–S5 linkers

Using our previously reported down-state model of the isolated KvAP VSD [24], we generated several down-state conformations of the KvAP channel using targeted molecular dynamics (TMD). One of them, described below, resulted in a closed-state conformation with a pore radius on the intracellular end of about 2 Å (Fig. 1E). The hydrated region within the channel vestibule is roughly 10 Å narrower in the closed conformation than in the open conformation, because the central region of the pore is partly occupied by the C-terminal half of S6 (Figs. 1E and 3). Therefore, a K^+ ion would have to dehydrate in order to enter the intracellular vestibule in the closed state. In contrast, in the open state, the ion would have to shed its water only at the selectivity filter, where it is more energetically favorable due to the inward facing backbone oxygens along the selectivity filter [43–46].

We used TMD (see Methods and Fig. 4) to drive the up-state configuration of the four VSDs toward a target configuration based on our previously reported down-state model of the isolated KvAP VSD [24]. Because the model does not prescribe the positions of the VSDs in the membrane plane with respect to the pore domain, we performed TMD simulations with four different VSD target states (Fig. 4A–E), only one of which resulted in a closed pore (Fig. 4F). Each had identical coordinates along the TM direction, but differed in its position relative to the center of the pore domain. Placement of the down-state VSDs at the same distance from the pore center as in the up-state conformation resulted in no pore closure (Fig. 4F). The only two possible displacements of the VSDs in the membrane plane are laterally, around the pore domain, or inwardly, toward the center of the pore domain (Fig. 4C–D). Either of these displacements alone produced a narrower, but still open pore, similar to the target without lateral displacement (Fig. 4F). In contrast, applying both lateral (clockwise) and inward displacements from the up-state (Fig. 4E) resulted in a pore domain with a pore radius profile similar to those observed in the closed conformations of the KcsA [43,44] and MlotiK1 [9] channel crystal structures (Fig. 5). The combination of lateral, radial, and downward VSD displacement produces a torque on the S4–S5 linkers and inward pressure on the intracellular end of S6, creating a packing environment that closes the pore when the VSDs are in the down-state conformation.

Our down-state model for the isolated VSD [24] was based primarily on a collection of experimental restraints obtained by mapping biotin–avidin accessibility data to the TM depths of 36 C_α atoms [25]. Ruta et al. [25] estimated from their accessibility data residue displacements along the membrane normal by using the location of the lipid bilayer interface as a fixed reference. For a quantitative comparison between these experimental restraints and our atomistic models of the full channel, we assumed that the interface of the thermally disordered lipid bilayer is described by the mean position and width of the carbonyl distributions (Fig. S1). In this reference frame, we find that both our open- and closed-state simulations are consistent with all the available biotin–avidin accessibility data on the KvAP VSD [25,42] (Fig. 6).

3.2. Voltage sensor motions and coupling to the pore domain

We do not know if the TMD-generated trajectory represents the true reaction coordinate for channel gating. Nevertheless, it is informative to characterize the conformational changes between the open and closed conformations through a comparison of our extensive unrestrained trajectories of the initial and final states (Figs. 7, 8, 9, S2). The displacements along the TM direction (Fig. 9) of S1 and S2 in the VSD, and the pore domain, except for the intracellular half of S6, are within the width of the carbonyl distribution (FWHM ~ 7 Å; Fig. S1). Consequently, these displacements do not participate in the channel conformational changes between the open and closed configurations. In contrast, the helical hairpins S3b–S4, the so-called paddle motif (Fig. 2), have been displaced 12 to 15 Å in the TM direction between the open and closed configurations but, as in the case of our isolated VSD model [24], they do not move as a rigid-body (Figs. 7, 9, and S2). The total charge displaced between the two conformations is 6.0 ± 0.3 *e* (Fig. S3 and Table S1).

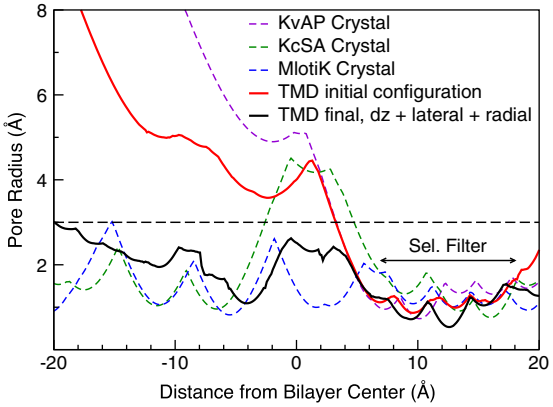

Fig. 5. The pore radius profiles of the KvAP channel open and closed TMD end-point configurations compared to those of the KvAP [4], KcsA [44], and Mlotik1 [9] crystal structures. The dashed black line represents the nominal radius of a hydrated K^+ ion. The profile of the closed-state model is similar to those of the closed-state KcsA and Mlotik1 structures.

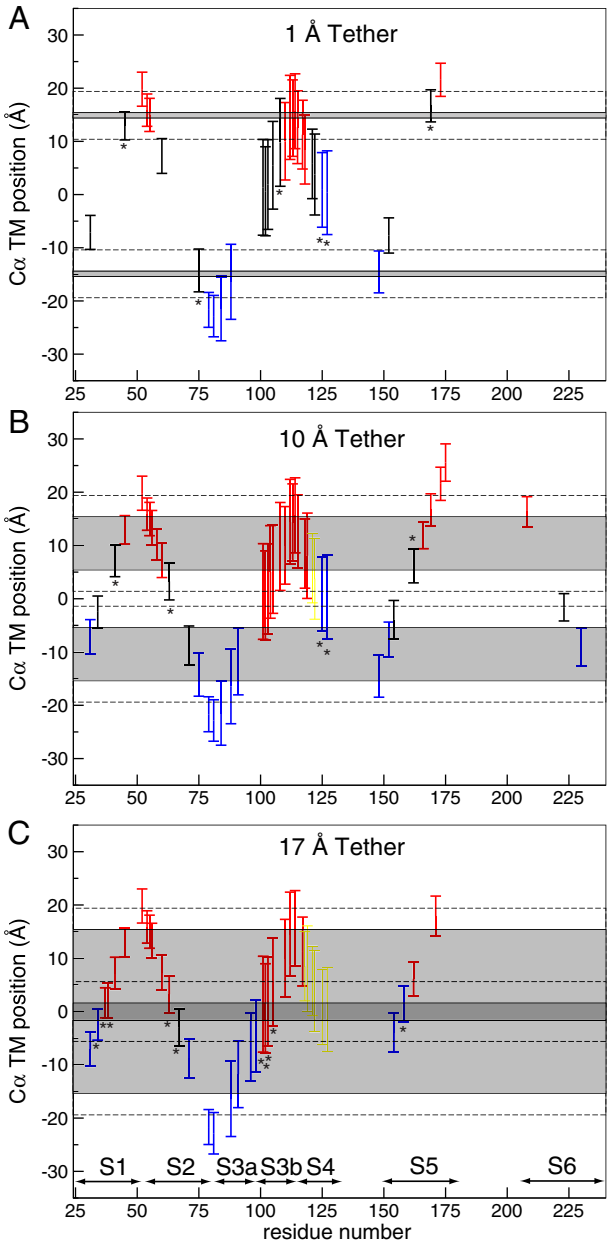

Fig. 6. Simulation-based interpretation of biotin–avidin accessibility data [25]. The minimum and maximum values of C_α positions along the TM direction are plotted against the effective length of three different biotin tethers (1, 10, and 17 Å). If the C_α range of a given residue falls within a given tether length of the bilayer edge (shaded gray regions), it is considered to be accessible to avidin on that side. If the C_α range overlaps both boxes, the residue is considered to be accessible from both sides. The means of the lipid carbonyl distributions (Fig. S2) determine the outer edge of each box (±15.4 Å); the inner edge corresponds to the effective tether length reported by Ruta et al. [25]. The C_α ranges are colored according to the reported accessibility: red, extracellular accessibility; blue, intracellular accessibility; yellow, accessibility from both sides; and black, inaccessibility. The dashed lines correspond to half of the carbonyl distribution full-width at half-maximum, and represent uncertainty in the bilayer thickness. Residues for which the simulation and experimental accessibility results disagree by more than the uncertainty in the bilayer thickness are marked with an asterisk.

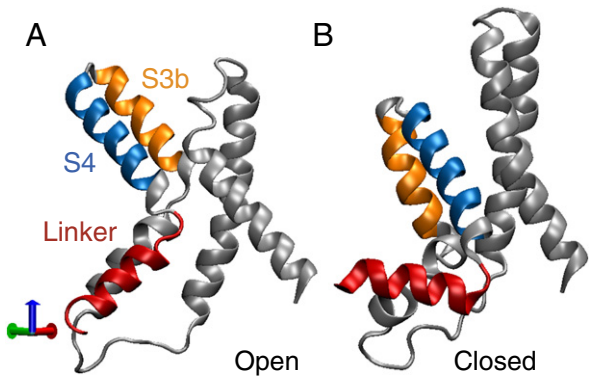

Fig. 7. Snapshots of the VSD in the (A) open and (B) closed conformations, with S3b (orange), S4 (blue), and the S4–S5 linker (red) highlighted. The S3b and S4 helices have assumed a more vertical orientation in the VSD down state, and the S4–S5 linker lays parallel to the interface in the closed channel.

Between the open and closed conformations, S4 pushes the N-terminal end of the S4–S5 linker downward (Figs. 7, 9). The motion of the S4–S5 linkers along the TM direction is best described as a tilt of 28° (Fig. S2) that produces full-contact surfaces with the polar region of the lipid bilayer. In addition, the motion of the VSDs in the membrane plane produces an inward rotation of the linker that brings it in full-contact with the C-terminal end of S6 (Fig. 8).

S6 is bent in the open state at G220 by approximately 50° from the pore axis and splays even further beyond G229 (see Fig. 10A,B and Table S2). This conformation forms a large hydrated intracellular cavity below the selectivity filter (Fig. 3A,B). In the closed state, the S6 intracellular halves have straightened at G220, and a hydrated, closed inner vestibule is formed; the pinching off of the vestibule is accompanied by a change in volume below the selectivity filter (Fig. 3C,D). The contact region between S4–S5 and the C-terminal end of S6, which lies immediately below G229, is displaced inward (Fig. 10B). Thus, both G220 and G229 appear to contribute to the gating mechanism in different ways. The bending dynamics at G229 allows for the formation of the C-terminal S6 helical bundle that produces a steric barrier on the intracellular side of the pore domain. The hinge-bending motion at G220 isolates the extracellular side from the gating dynamics, and appears to facilitate the formation of the inner vestibule under the selectivity filter, thereby providing an energetically favorable environment for ions located in the selectivity filter [44,47].

In both the open and closed conformations, contacts between S1 and the pore domain on the extracellular side appear to be important for maintaining the VSDs in an upright position. The specific contacts, first produced by equilibration with harmonic restraints in the up-state conformation (Methods), correspond to a cysteine cross-link between T47 (S1 helix) and V183 (P-helix) reported by Lee et al. [40] for KvAP. Lee et al. [40] also found, using statistical coupling analysis over a large sample of Kv channel sequences, that a set of residues located at the extracellular ends of S1 and the pore domain form an evolutionarily conserved interface. To determine whether this interface acts as an anchor during gating, we performed a TMD simulation using the same target location of the VSD that successfully closed the pore, but used as a starting point an equilibrated configuration of the channel based on the original model of Lee et al. [4], in which there are no contacts between S1 and the pore domain (Fig. S4). The down state generated in this simulation exhibits a pore radius profile intermediate between the open and closed states (Fig. S4C), suggesting that the S1-pore-domain interface likely plays a role in stabilizing the VSD during activation.

3.3. Voltage sensor interactions determine S4 secondary structure

Salt-bridge formation between the basic side chains in S4 and a group of conserved acidic side chains in S1 through S3 are crucial to the folding, stability, and function of the VSD [48–51]. Salt-bridge formation between lipid phosphates and the S4 charges has also been reported as important for VSD stability and function [18–20,52,53].

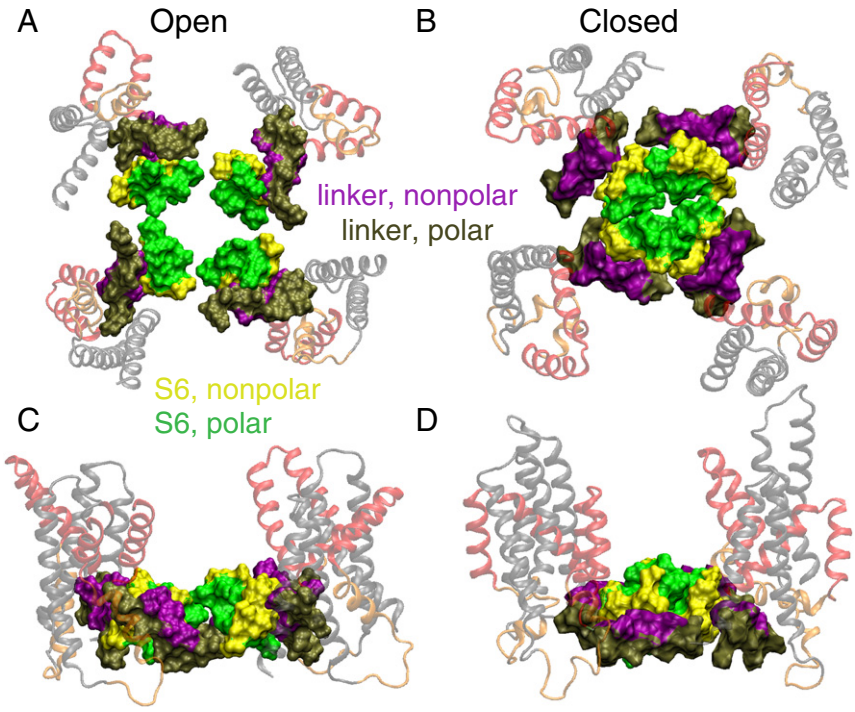

Fig. 8. Contacts between S6 and the S4–S5 linker helices. The VSDs are shown in transparent ribbon and colored as in Fig. 1. The S4–S5 linker and the intracellular end of S6 (residues 229–240) are shown as a molecular surface and colored by polarity (polar linker residues, brown; nonpolar linker, purple; polar S6, green; and nonpolar S6, yellow). The four panels are snapshots of the open (A,C) and closed (B,D) states taken from extracellular and side views, respectively. Both the linker and S6 are clearly divided into hydrophobic and polar surfaces; the polar surfaces face the aqueous environment (bilayer interface and pore cavity), while the nonpolar faces form a hydrophobic interface between the linker and S6 helices.

The salt-bridge interactions in both the open and closed states are summarized in Table S3. Although there are common features among the salt-bridge networks in the closed state, each VSD displays distinctive salt-bridge configurations. In contrast, the solvation of the S4 arginines is much more consistent across subunits in the up-state, probably because in this state fewer charged residues face the VSD interior.

No explicit constraints were placed on the backbone structure. Nevertheless, we observed that the S4 backbone undergoes an α- to 3_{10}-helix transition on the extracellular half (roughly from residues 117 to 124) of all four subunits during the TMD portion of the simulation (Fig. S5). The 3_{10}-helix conformation places the S4 arginines, which occur at every third sequence position, on the same face of the helix, thus allowing all of the Arg side chains to form salt-bridge

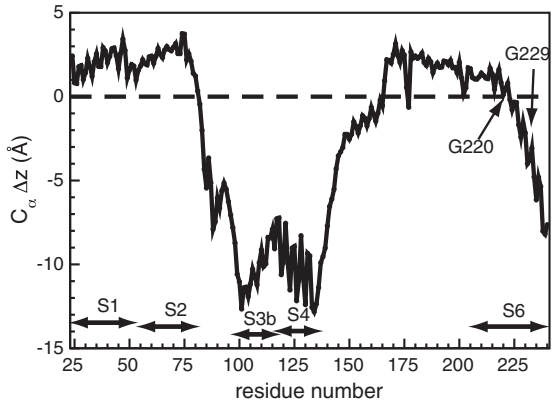

Fig. 9. Net transmembrane displacement. The difference between the average C_α positions in the open- and closed-state simulations, averaged over the last 200 ns of each trajectory. The motion is confined largely to the S3b–S4 helices and the intracellular half of S6.

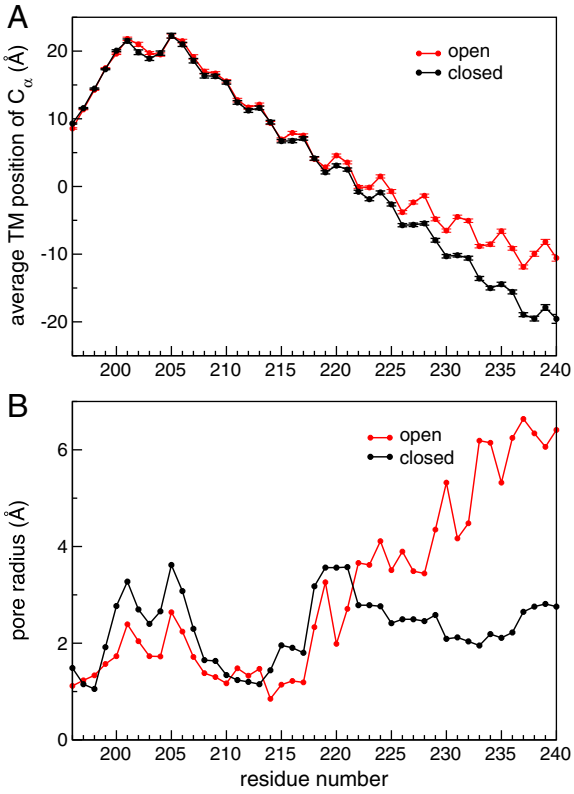

Fig. 10. Hinging along the S6 helix. (A) Average C_α position with respect to the bilayer center as a function of sequence position. (B) Pore radius as a function of sequence position. The data are similar for both the open and closed simulations until around G220, below which the open-state pore begins to splay open with respect to the closed state. The difference is even more pronounced below G229.

interactions with acidic residues. In contrast, R1 and R2 in the VSD up-state are exposed to the bilayer interface and face away from the interior of the VSD, permitting S4 to retain the α-helical conformation of the initial configuration. In the two subunits in which R4 maintains a salt-bridge with D72, the 3_{10}-helix secondary structure persists throughout much of the simulation, while in those subunits where R4 is facing the intracellular interface without a protein salt-bridge partner, the down-state secondary structure quickly reverts to an α-helix.

4. Discussion

To gain insights into the nature of the mechanical coupling between the VSDs and the pore domain, we have generated in two steps a closed-state model of the KvAP channel based entirely on the motion of the VSDs. First, we modeled a down-state of the isolated VSD using a methodology similar to that employed in structural refinement by NMR, specifically, mapping available experimental data onto position and distance restraints, followed by an unrestrained MD simulation to optimize the resulting conformation [24]. Second, we used TMD to guide the four VSDs toward the down-state conformation, starting from a model of the full channel in an open state. No restraint forces were applied to the pore domain during the TMD simulation. We tested several target configurations, each with different displacements of the VSDs in the membrane plane, to find the combination that would lead to the closing of the channel. When probing the possible two-dimensional displacements between target and initial configurations, we used the circumference described by the projection of the pore domain on the membrane plane to define the possible directions of motion, and we limited the magnitude of displacements along either direction to ~3 Å. Thus, beginning from experimentally derived restraints, we have systematically explored the relevant degrees of freedom of the VSDs. We conclude that, in addition to motions along the TM direction, small in-plane displacements of the VSDs are necessary to achieve a fully closed conformation of the pore domain.

Our closed pore domain exhibits features found in the closed-state crystal structure of other ion channels [6,9,10,43,44,54]: a tightly packed inner helix bundle on the intracellular end, and a hydrated inner vestibule, as seen in the crystal structures of KcsA [43,44] and NaK [10]. Our closed state conformation is also consistent with a cysteine cross-linking tetramerization assay that distinguishes between the open and closed conformation of the KvAP pore domain reported recently by Zheng et al. [55]. Cysteine mutants at the position of closest approach between subunits in the region of the activation gate in the KvAP crystal structure (T225) were found to form tetramers in more than 85% of the channels in the closed state, and in less than 50% in the open state [55]. Consistent with these results, we find minimum average T225 Cβ-Cβ distances between opposite subunit pairs of 6.2 ± 0.4 Å and 7.8 ± 0.4 Å in the closed state and 9.2 ± 0.5 Å and 9.4 ± 0.5 Å in the open state.

Our modeling suggests that coupling between the motions of the VSDs and the closing of the pore domain occurs through the formation of a full-contact hydrophobic interface between the S4–S5 linker and the intracellular end of S6. Our model is thus consistent with functional [15–17] and crystallographic [1,2] data that identify the linker-S6 interface as a key structural element involved in Kv channel gating. The crystal structure of the Kv1.2 paddle-chimera channel exhibits close contacts between S1 and the pore domain [1]. The existence of this interface is consistent with functional data in eukaryotic channels [40] and has been inferred in KvAP from cross-linking [40] and LRET data [56]. As previously suggested, we find that such a feature may be required for the VSDs to transmit force to the S4–S5 linkers [1,40]. Taken together, these results suggest that modular nature of the Kv channels relies on the occurrence of these interfaces between the VSDs and the pore domain. Consistent with the notion that the activation gating mechanism of tetrameric ion channels is independent of the nature of the gating stimulus, we find that the VSDs steer the S4–S5 linkers to mirror the expected motions of the pore domain suggested by EPR [8] and metal-binding [57,58] accessibility assays, crystallography [10,54], as well as normal mode analysis [59–61].

The available crystal structures of ion channel pore domains identify two putative hinge-bending sites in the inner helix (S6 in Kv channels) that appear to be implicated in activation gating: a highly conserved Gly (G220 in KvAP) and a second bending site at a Gly or Pro residue (G229 in KvAP and the P-X-P motif in the Kv1–Kv4 subfamilies). Although both features are present in the sequence of most potassium ion channels, they have been considered as leading to mutually exclusive mechanisms of gating [11,12]. In contrast, our results suggest that these two features may complement each other, as suggested previously [7,60,61]. The bend at G229 clearly plays the main role in the formation of the S6 helical bundle that constitutes the activation gate, but the associated conformational change starts at G220, allowing the formation of a hydrated inner vestibule while keeping the extracellular region of the pore relatively rigid. Because we do not know if the pathway between the open and closed states generated by our TMD simulation is the correct reaction coordinate, we cannot draw definitive conclusions concerning the interplay between the bending at the two conserved glycines. However, detailed modeling of the open-to-closed transition in KcsA suggests that bending of S6 at these sites may constitute the initial and final stages that lead to the open and closed conformations [61].

A hydrophobic interface between the S4–S5 linker and the S6 helices is seen in the structure of NavAb [6], which features apparently activated VSDs and a closed pore domain. However, while the conservation of the linker-S6 interface suggests that those contacts are important for gating in both Kv and Nav channels, the stark difference in their S6 sequences suggests that the actual gating motion of S6 above the point of contact with the linker is different in Nav and Kv channels. The NavAb S6 sequence is almost entirely hydrophobic, contains no Gly residues, and only a single Pro residue located approximately 1–2 helical turns from the extracellular bilayer interface. Thus, the dual-hinge bending mechanism suggested in this work for Kv channels is not employed by the Nav channel.

Previously, Pathak et al. [62] reported a de novo atomistic model of the closed state of the Kv1.2 channel based on extensive voltage-clamp fluorescence data, studies of the omega current pathway in *Shaker* mutants [63,64], and accessibility data on the S6 intracellular side [57,65]. The overall conformation of the closed pore domain and the net displacement of the S4–S5 linkers on the membrane plane are similar to those reported here, although the longer S4 segment in Kv1.2 appears to place the S4–S5 linkers in full contact with the polar region of the lipid bilayer in both states.

We calculated a total gating charge displacement of 6.0 ± 0.3 *e*, which is less than the widely cited 12.3–13.6 *e* reported for the *Shaker* channel [49,66,67], but comparable to the 7.5 *e* reported for the *Shab* channel [68]. Gating charge displacement appears to be very sensitive to amino acid sequence. For example, rat Kv2.1 and *Shab* have very high sequence identity, yet their gating charge values, as estimated by the limiting-slope method, differ by 5 *e* (12.5 *e* and 7.5 *e*, respectively) [68]. The calculated values of gating charge from atomistic modeling are very sensitive to the S4 Arg side chain configurations [69,70]. For example, Khalili-Araghi et al. [69] initially calculated a gating charge of 10.3 *e* after 150 ns of simulation of the Kv1.2 Pathak et al. [62] models under an applied potential, but after steering R1 ~ 2.5 Å toward the intracellular side of the membrane to encourage a salt bridge between R1 and E226 (D62 in KvAP), the calculated value increased to 12.7 *e*. Similarly, Delemotte et al. [70], reported a charge displacement of 4.8 *e* in a 2.2 μs simulation of Kv1.2 under an applied potential, and then generated additional conformational changes by applying harmonic restraints to the six basic residues on S4 to encourage the formation of specific salt-bridges, leading to

two additional conformational states and a final gating charge value of 12.8 *e* [70].

In KvAP, the paddle motif is shorter than in Kv1 channels, which might account for a smaller value of net charge displaced during gating. The KvAP VSD also lacks the so-called gating charge transfer center, a structural feature in eukaryotic Kv VSDs formed by a highly-conserved Phe side chain and two acidic side chains, that has been suggested to catalyze the crossing of basic side chains in S4 through the membrane electric field during voltage-dependent activation [71]. This same highly conserved Phe side chain has also been suggested to define the membrane dielectric barrier through the VSD [72]. The net displacement of the S4–S5 linker along the TM direction (Figs. 7 and S2), as well as the large contribution of R6 to the gating charge (Fig. S3), suggest that the details of the conformational changes in the KvAP VSD during voltage-dependent activation may differ from those in eukaryotic VSDs.

Overall, VSD salt-bridge interactions appear to be more uniform in the open state than in the closed state according to our modeling of the KvAP channel. Similar results have been reported in MD simulations of the Kv1.2 channel in the closed state [69,70]. Atomistic MD trajectories of Kv channels in lipid bilayers on the 100-ns time scale are likely not long enough to sample these interactions completely. However, it is possible that the results of such simulations provide a reasonable qualitative description of the difference between the open and closed conformations. Assuming that VSD salt-bridge interactions shape the activation landscape, these results would be consistent with a proposed energy-landscape interpretation of gating kinetics in *Shaker* [73] that suggest that the channel open state would be in a narrower potential well in comparison to the resting state. Such a result would be also consistent with the suggestion that the Kv channel crystal structures represent a relaxed state distinct from the transient activated/open state [74].

Acknowledgements

This work was supported by grants from the NIGMS and NINDS of the National Institutes of Health (GM74737 to S.H.W. and Program Project GM86685 to S.H.W. and D.J.T), and the National Science Foundation (CHE-0750175 to D.J.T). The computations were enabled in part by the NSF through TeraGrid resources provided by the TACC at UT Austin, and the University of California Shared Research Computing Services (SharCS) pilot project.

Appendix A. Supplementary data

Supplementary data to this article can be found online at doi:10.1016/j.bbamem.2012.02.029.

References

[1] S.B. Long, X. Tao, E.B. Campbell, R. Mackinnon, Atomic structure of a voltage-dependent K^+ channel in a lipid membrane-like environment, Nature 450 (2007) 376–382.
[2] S.B. Long, E.B. Campbell, R. MacKinnon, Voltage sensor of Kv1.2: structural basis of electromechanical coupling, Science 309 (2005) 903–908.
[3] S.B. Long, E.B. Campbell, R. MacKinnon, Crystal structure of a mammalian voltage-dependent Shaker-family K^+ channel, Science 309 (2005) 897–903.
[4] S.-Y. Lee, A. Lee, J. Chen, R. MacKinnon, Structure of the KvAP voltage-dependent K^+ channel and its dependence on the lipid membrane, Proc. Natl. Acad. Sci. U. S. A. 102 (2005) 15441–15446.
[5] Y.X. Jiang, A. Lee, J.Y. Chen, V. Ruta, M. Cadene, B.T. Chait, R. MacKinnon, X-ray structure of a voltage-dependent K^+ channel, Nature 423 (2003) 33–41.
[6] J. Payandeh, T. Scheuer, N. Zheng, W.A. Catterall, The crystal structure of a voltage-gated sodium channel, Nature 475 (2011) 353–358.
[7] Y.X. Jiang, A. Lee, J.Y. Chen, M. Cadene, B.T. Chait, R. MacKinnon, The open pore conformation of potassium channels, Nature 417 (2002) 523–526.
[8] E. Perozo, D.M. Cortes, L.G. Cuello, Structural rearrangements underlying K^+-channel activation gating, Science 285 (1999) 73–78.
[9] G.M. Clayton, S. Altieri, L. Heginbotham, V.M. Unger, J.H. Morais-Cabral, Structure of the transmembrane regions of a bacterial cyclic nucleotide-regulated channel, Proc. Natl. Acad. Sci. U. S. A. 105 (2008) 1511–1515.
[10] A. Alam, Y. Jiang, Structural analysis of ion selectivity in the NaK channel, Nature Struct. Mol. Biol. 16 (2009) 35–41.
[11] K.J. Swartz, Towards a structural view of gating in potassium channels, Nat. Rev. Neurosci. 5 (2004) 905–916.
[12] F. Tombola, M.M. Pathak, E.Y. Isacoff, How does voltage open an ion channel? Annu. Rev. Cell Dev. Biol. 22 (2006) 23–52.
[13] E. Magidovich, O. Yifrach, Conserved gating hinge in ligand- and voltage-dependent K + channels, Biochemistry 43 (2004) 13242–132476.
[14] S. Ding, L. Ingleby, C.A. Ahern, R. Horn, Investigating the putative glycine hinge in shaker potassium channel, J. Gen. Physiol. 126 (2005) 213–226.
[15] Z. Lu, A.M. Klem, Y. Ramu, Coupling between voltage sensors and activation gate in voltage-gated K^+ channels, J. Gen. Physiol. 120 (2002) 663–676.
[16] Z. Lu, A.M. Klem, Y. Ramu, Ion conduction pore is conserved among potassium channels, Nature 413 (2001) 809–813.
[17] A.J. Labro, A.L. Raes, A. Grottesi, D. Van Hoorick, M.S. Sansom, D.J. Snyders, Kv channel gating requires a compatible S4–S5 linker and bottom part of S6, constrained by non-interacting residues, J. Gen. Physiol. 132 (2008) 667–680.
[18] S. Chakrapani, L.G. Cuello, D.M. Cortes, E. Perozo, Structural dynamics of an isolated voltage-sensor domain in a lipid bilayer, Structure 16 (2008) 398–409.
[19] L.G. Cuello, D.M. Cortes, E. Perozo, Molecular architecture of the KvAP voltage-dependent K^+ channel in a lipid bilayer, Science 306 (2004) 491–495.
[20] D. Krepkiy, M. Mihailescu, J.A. Freites, E.V. Schow, D.L. Worcester, K. Gawrisch, D.J. Tobias, S.H. White, K.J. Swartz, Structure and hydration of membranes embedded with voltage-sensing domains, Nature 462 (2009) 473–479.
[21] I.S. Ramsey, M.M. Moran, J.A. Chong, D.E. Clapham, A voltage-gated proton-selective channel lacking the pore domain, Nature 440 (2006) 1213–1216.
[22] M. Sasaki, M. Takagi, Y. Okamura, A voltage-sensor domain protein is a voltage-gated proton channel, Science 312 (2006) 589–592.
[23] Y. Murata, H. Iwasaki, M. Sasaki, K. Inaba, Y. Okamura, Phosphoinositide phosphatase activity coupled to an intrinsic voltage sensor, Nature 435 (2005) 1239–1243.
[24] E.V. Schow, J.A. Freites, K. Gogna, S.H. White, D.J. Tobias, Down-state model of the voltage-sensing domain of a potassium channel, Biophys. J. 98 (2010) 2857–2866.
[25] V. Ruta, J. Chen, R. MacKinnon, Calibrated measurement of gating-charge arginine, Cell 123 (2005) 463–475.
[26] J.C. Phillips, B. Braun, W. Wang, J. Gumbart, E. Tajkhorshid, E. Villa, C. Chipot, R.D. Skeel, L. Kalé, K. Schulten, Scalable molecular dynamics with NAMD, J. Comput. Chem. 26 (2005) 1781–1802.
[27] A.D. MacKerell Jr., D. Bashford, M. Bellott, R.L. Dunbrack Jr., J.D. Evanseck, M.J. Field, S. Fischer, J. Gao, H. Guo, S. Ha, D. Joseph-McCarthy, L. Kuchnir, K. Kuczera, F.T.K. Lau, C. Mattos, S. Michnick, T. Ngo, D.T. Nguyen, B. Prodhom, W.E. Reiher III, B. Roux, M. Schlenkrich, J.C. Smith, R. Stote, J. Straub, M. Watanabe, J. Wiórkiewicz-Kuczera, D. Yin, M. Karplus, All-atom empirical potential for molecular modeling and dynamics studies of proteins, J. Phys. Chem. B 102 (1998) 3586–3616.
[28] J.B. Klauda, B.R. Brooks, A.D. MacKerell Jr., R.M. Venable, R.W. Pastor, An ab initio study on the torsional surface of alkanes and its effect on molecular simulations of alkanes and a DPPC bilayer, J. Phys. Chem. B 109 (2005) 5300–5311.
[29] W.L. Jorgensen, J. Chandrasekhar, J.D. Madura, R.W. Impey, M.L. Klein, Comparison of simple potential functions for simulating liquid water, J. Chem. Phys. 79 (1983) 926–935.
[30] U. Essmann, L. Perera, M.L. Berkowitz, T. Darden, H. Lee, L.G. Pedersen, A smooth particle mesh Ewald method, J. Chem. Phys. 103 (1995) 8577–8593.
[31] T. Darden, D. York, L. Pedersen, Particle mesh Ewald: an *N*•log(*N*) method for Ewald sums in large systems, J. Chem. Phys. 98 (1993) 10089–10092.
[32] H. Grubmüller, H. Heller, A. Windemuth, K. Schulten, Generalized Verlet algorithm for efficient molecular dynamics simulations with long-range interactions, Mol. Simul. 6 (1991) 121–142.
[33] J.-P. Ryckaert, G. Ciccotti, H.J.C. Berendsen, Numerical integration of the Cartesian equations of motion of a system with constraints: molecular dynamics of *n*-alkanes, J. Comput. Phys. 23 (1977) 327–341.
[34] S. Miyamoto, P. Kollman, An analytical version of the SHAKE and RATTLE algorithm for rigid water models, J. Comput. Chem. 13 (1992) 952–962.
[35] W. Humphrey, W. Dalke, K. Schulten, VMD: visual molecular dynamics, J. Mol. Graph. 14 (1996) 33–38.
[36] G.J. Martyna, D.J. Tobias, M.L. Klein, Constant-pressure molecular-dynamics algorithms, J. Chem. Phys. 101 (1994) 4177–4189.
[37] S.E. Feller, Y. Zhang, R.W. Pastor, B.R. Brooks, Constant pressure molecular dynamics simulation: the Langevin piston method, J. Chem. Phys. 103 (1995) 4613–4621.
[38] O.S. Smart, J.G. Neduvelil, X. Wang, B.A. Wallace, M.S. Sansom, HOLE: a program for the analysis of the pore dimensions of ion channel structural models, J. Mol. Graph. 14 (1996) 354–360.
[39] B.R. Brooks, CHARMM: the biomolecular simulation program, J. Comput. Chem. 30 (2009) 1545–1614.
[40] S.-Y. Lee, A. Banerjee, R. MacKinnon, Two separate interfaces between the voltage sensor and pore are required for the function of voltage-dependent K^+ channels, PLoS Biol. 7 (2009) 0676–0686.
[41] W. Treptow, M. Tarek, M.L. Klein, Initial response of the potassium channel voltage sensor to a transmembrane potential, J. Am. Chem. Soc. 131 (2009) 2107–2109.
[42] A. Banerjee, R. MacKinnon, Inferred motions of the S3a helix during voltage-dependent K^+ channel gating, J. Mol. Biol. 381 (2008) 569–580.

[43] Y. Zhou, J.H. Morais-Cabral, A. Kaufman, R. MacKinnon, Chemistry of ion coordination and hydration revealed by a K^+ channel–Fab complex at 2.0 Å resolution, Nature (2001) 43–48.
[44] D.A. Doyle, J.M. Cabral, R.A. Pfuetzner, A.L. Kuo, J.M. Gulbis, S.L. Cohen, B.T. Chait, R. MacKinnon, The structure of the potassium channel: molecular basis of K^+ conduction and selectivity, Science 280 (1998) 69–77.
[45] J.H. Morais-Cabral, Y. Zhou, R. MacKinnon, Energetic optimization of ion conduction rate by the K^+ selectivity filter, Nature 414 (2001) 37–42.
[46] S.Y. Noskov, S. Bernèche, B. Roux, Control of ion selectivity in potassium channels by electrostatic and dynamic properties of carbonyl ligands, Nature 431 (2004) 830–834.
[47] A.N. Thompson, I. Kim, T.D. Panosian, T.M. Iverson, T.W. Allen, C.M. Nimigean, Mechanism of potassium-channel selectivity revealed by Na^+ and Li^+ binding sites within the KcsA pore, Nature Struct. Mol. Biol. 16 (2009) 1317–1324.
[48] D.M. Papazian, X.M. Shao, S.-A. Seoh, A.F. Mock, Y. Huang, D.H. Wainstock, Electrostatic interactions of S4 voltage sensor in Shaker K^+ channel, Neuron 14 (1995) 1293–1301.
[49] S.A. Seoh, D. Sigg, D.M. Papazian, F. Bezanilla, Voltage-sensing residues in the S2 and S4 segments of the Shaker K^+ channel, Neuron 16 (1996) 1159–1167.
[50] S.K. Tiwari-Woodruff, C.T. Schulteis, A.F. Mock, D. Papazian, Electrostatic interactions between transmembrane segments mediate folding of *Shaker* K^+ channel subunits, Biophys. J. 72 (1997) 1489–1500.
[51] L. Zhang, Y. Sato, T. Hessa, G. von Heijne, J.-K. Lee, I. Kodama, M. Sakaguchi, N. Uozumi, Contribution of hydrophobic and electrostatic interactions to the membrane integration of the Shaker K^+ channel voltage sensor domain, Proc. Natl. Acad. Sci. U. S. A. 104 (2007) 8263–8268.
[52] Y. Ramu, Y. Xu, Z. Lu, Enzymatic activation of voltage-gated potassium channels, Nature 442 (2006) 696–699.
[53] D. Schmidt, Q.-X. Jiang, R. MacKinnon, Phospholipids and the origin of cationic gating charges in voltage sensors, Nature 444 (2006) 775–779.
[54] A. Alam, Y. Jiang, High-resolution structure of the open NaK channel, Nature Struct. Mol. Biol. 16 (2009) 30–34.
[55] H. Zheng, W. Liu, L.Y. Anderson, Q.-X. Jiang, Lipid-dependent gating of a voltage-gated potassium channel, Nat. Commun. 250 (2011) 1–9.
[56] J. Richardson, R. Blunck, P. Ge, P.R. Selvin, F. Bezanilla, D.M. Papzian, A.M. Correa, Distance measurements reveal a common topology of prokaryotic voltage-gated ion channels in the lipid bilayer, Proc. Natl. Acad. Sci. U. S. A. 103 (2006) 15865–15870.
[57] D. del Camino, G. Yellen, Tight steric closure at the intracellular activation gate of a voltage-gated K^+ channel, Neuron 32 (2001) 649–656.
[58] S.M. Webster, D. del Camino, J.P. Dekker, G. Yellen, Intracellular gate opening in Shaker channels defined by high-affinity metal bridges, Nature 428 (2004) 864–868.
[59] I.H. Shrivastava, I. Bahar, Common mechanism of pore opening shared by five differenct potassium channels, Biophys. J. 90 (2006) 3929–3940.
[60] Y. Shen, Y. Kong, J. Ma, Intrinsic flexibility and gating mechanism of the potassium channel KcsA, Proc. Natl. Acad. Sci. U. S. A. 99 (2002) 1949–1953.
[61] G.V. Miloshevsky, P.C. Jordan, Open-state conformation of the KcsA K+ channel: Monte Carlo normal mode following simulations, Structure 15 (2007) 1654–1662.
[62] M.M. Pathak, V. Yarov-Yarovoy, G. Agarwal, B. Roux, P. Barth, S. Kohout, F. Tombola, E.Y. Isacoff, Closing in on the resting state of the Shaker K^+ channel, Neuron 56 (2007) 124–140.
[63] F. Tombola, M.M. Pathak, P. Gorostiza, E.Y. Isacoff, The twisted ion-permeation pathway of a resting voltage-sensing domain, Nature 445 (2007) 546–549.
[64] F. Tombola, M.M. Pathak, E.Y. Isacoff, Voltage-sensing arginines in a potassium channel permeate and occlude cation-selective pores, Neuron 45 (2005) 379–388.
[65] D. del Camino, M. Kanevsky, G. Yellen, Status of the intracellular gate in the activated-not-open state of shaker K^+ channels, J. Gen. Physiol. 126 (2005) 419–428.
[66] S.K. Aggarwal, R. MacKinnon, Contribution of the S4 segment to gating charge in the *Shaker* K^+ channel, Neuron 16 (1996) 1169–1177.
[67] N.E. Schoppa, K. McCormack, M.A. Tanouye, F.J. Sigworth, The size of gating charge in wild-type and mutant *Shaker* potassium channels, Science 255 (1992) 1712–1715.
[68] L.D. Islas, F.J. Sigworth, Voltage sensitivity and gating charge in Shaker and Shab family potassium channels, J. Gen. Physiol. 114 (1999) 723–741.
[69] F. Khalili-Araghi, V. Jogini, V. Yarov-Yarovoy, E. Tajkhorshid, B. Roux, K. Schulten, Calculation of the gating charge for the Kv1.2 voltage-activated potassium channel, Biophys. J. 98 (2010) 2189–2198.
[70] L. Delemotte, M. Tarek, M.L. Klein, C. Amaral, W. Treptow, Intermediate states of the Kv1.2 voltage sensor from atomistic molecular dynamics simulations, Proc. Natl. Acad. Sci. U. S. A. 108 (2011) 6109–6114.
[71] X. Tao, A. Lee, W. Limapichat, D.A. Dougherty, R. MacKinnon, A gating charge transfer center in voltage sensors, Science 328 (2010) 67–73.
[72] J.J. Lacroix, F. Bezanilla, Control of a final gating charge transition by a hydrophobic residue in the S2 segment of a K^+ channel voltage sensor, Proc. Natl. Acad. Sci. U. S. A. 108 (2011) 6444–6449.
[73] D. Sigg, F. Bezanilla, A physical model of potassium channel activation: from energy landscape to gating kinetics, Biophys. J. 84 (2003) 3703–3716.
[74] C.A. Villalba-Galea, W. Sandtner, D.M. Starace, F. Bezanilla, S4-based voltage sensors have three major conformations, Proc. Natl. Acad. Sci. U. S. A. 105 (2008) 17600–17607.